



Ab initio molecular dynamics study of prebiotic production processes of organic compounds at meteorite impacts on ocean

Shimamura, Kohei
Shimojo, Fuyuki
Nakano, Aiichiro
Tanaka, Shigenori

(Citation)

Journal of Computational Chemistry, 40(2):349-359

(Issue Date)

2019-01-15

(Resource Type)

journal article

(Version)

Accepted Manuscript

(Rights)

© 2018 Wiley Periodicals, Inc. This is the peer reviewed version of the following article: [Journal of Computational Chemistry, 40(2):349-359, 2019], which has been published in final form at <https://doi.org/10.1002/jcc.25606>. This article may be used for non-commercial purposes in accordance with Wiley Terms and Conditions for Use of...

(URL)

<https://hdl.handle.net/20.500.14094/90006452>



Ab Initio Molecular Dynamics Study of Prebiotic Production Processes of Organic Compounds at Meteorite Impacts on Ocean

Kohei Shimamura¹ | Fuyuki Shimojo² | Aiichiro Nakano³ | Shigenori Tanaka¹

¹Graduate School of System Informatics, Kobe University, 1-1 Rokkodai, Nada-ku, Kobe 657-8501, Japan

²Department of Physics, Kumamoto University, 2-39-1 Kurokami, Chuo-ku, Kumamoto 860-8555, Japan

³Collaboratory for Advanced Computing and Simulations, Department of Physics & Astronomy, Department of Computer Science, Department of Chemical Engineering & Materials Science, and Department of Biological Sciences, University of Southern California, Los Angeles, CA 90089-0242, USA

Correspondence

Kohei Shimamura and Shigenori Tanaka
Graduate School of System Informatics,
Kobe University, 1-1 Rokkodai, Nada-ku,
Kobe 657-8501, Japan
Email: shimamura@port.kobe-u.ac.jp,
tanaka2@kobe-u.ac.jp

Funding information

The financial supports of KAKENHI,
Grant/Award Number: 16K17782,
17H06353, 18K03825, and 26460035

Recent experiments concerning prebiotic materials syntheses suggest that the iron-bearing meteorite impacts on ocean during Late Heavy Bombardment provided abundant organic compounds associated with biomolecules such as amino acids and nucleobases. However, the molecular mechanism of a series of chemical reactions to produce such compounds is not well understood. In this study, we simulate the shock compression state of a meteorite impact for a model system composed of CO₂, H₂O, and metallic iron slab by *ab initio* molecular dynamics combined with multi-scale shock technique, and clarify possible elementary reaction processes up to production of organic compounds. The reactions included not only pathways similar to the Fischer-Tropsch process known as an important hydrocarbon synthesis in many planetary processes but also those resulting in production of a carboxylic acid. It is also found that bicarbonate ions formed from CO₂ and H₂O participated in some forms in most of these observed elementary reaction processes. These findings would deepen the understanding of the full range of chemical reactions that could occur in the meteorite impact events.

KEYWORDS

Ab initio molecular dynamics, Multi-scale shock technique,
Meteorite impacts, Shock waves, Organic compounds

1 | INTRODUCTION

The early Earth was covered with the redox-neutral environment composed mainly of CO_2 , N_2 , and H_2O , which was harsh for birth of life. [1, 2] However, since traces of life have been discovered from the strata of 3.7 billion years ago, [3, 4] some important processes providing a reducing environment capable of production of organic compounds such as amino acids should have existed in the Earth at least 3.7 billion years ago. While various production mechanisms of the organic compounds have been discussed so far, the production via meteorite impacts on ancient ocean has recently attracted much attention. [5, 6, 7, 8] From 4.1 to 3.8 or 3.7 billion years ago, it is believed there was a period during which a large amount of meteorites came to the Earth, called late heavy bombardment (LHB). [9, 10, 11] While a lot of discussions have been made as to what type of meteorite had arrived during the LHB period, the present study focuses on the possibility of inflow of meteorites containing abundant metallic iron toward Earth because various biomolecules such as amino acids could be produced by meteorite collision with metallic iron being contained. This relevance can be assessed by the study of Bottke *et al.* [11] They suggested that impactors during the LHB period originated from the E-belt existing in the periphery of the Mars-crossing zone. Majority of the E-belt asteroids would have acquired orbits similar to those of the Hungaria asteroids, which contain a large amount of metallic iron. The metallic iron would have acted as a strong reductant for the oxidized substances on the early Earth. Based on these insights, Nakazawa and Furukawa *et al.* began to perform shock experiments in 2005, [5, 6, 7, 8] simulating the impacts of iron-bearing meteorites on ancient ocean under the redox-neutral environment. In 2009, [6] they succeeded in producing four types of proteinaceous amino acids from N_2 , NH_3 , H_2O , carbon amorphous, and metallic iron as starting materials. Furthermore, in 2015, [8] they found two kinds of nucleobases, in addition to nine kinds of amino acids, where bicarbonate (HCO_3^-) was used as a carbon source instead of the carbon amorphous. From these experimental results, it has been suggested that the ocean collisions of the meteorite would be quite important as events that provided a large amount of organic biological substances on the early Earth.

Their hypothesis brings about an expectation that meteorite impacts at the LHB period was closely related to the origin of life, but the production mechanism of the biomolecules is not well understood. Atomistic investigation is indispensable to clarify the conditions necessary for the generation of the remaining molecular building blocks (e.g. the remaining eleven kinds of amino acids that have not yet been detected in the experiment [8]). In order to obtain the fundamental insights from the atomistic point of view, therefore, we have investigated the production mechanisms using *ab initio* molecular dynamics simulation combined with multi-scale shock technique [12, 13] (MSST-AIMD). Through this attempt, we would like to find heterogeneous chemical reactions due to shock waves which are difficult to analyze in chemical equilibrium theory. We have thus far reported the results on the production process of NH_3 , [14, 15] which is an important reductive nitrogen source of biomolecules. We have simulated a shock wave generated by a meteorite impact which hits a model system consisting of N_2 and H_2O of the primitive ocean, and meteoritic iron. [14] We clarified that NH_3 could be produced by multiple atomistic mechanisms during impact compression for several picoseconds. [15]

In this work, we report the results of MSST-AIMD simulations, where shock waves hit the computational model consisting of CO_2 , H_2O , and meteoritic iron. Although many ions such as Na^+ , Mg^{2+} , and Cl^- are dissolved in the ocean, this study models seawater with pure water, ignoring the influence of these ions. While various shapes are conceivable as the structure of metallic iron, this study focuses on only the slab structure because of its simplicity. In addition, we used the slab with heterogeneous surfaces resembling those of the meteorite (see Fig. 1). The purpose of the simulations

was to elucidate what kinds of organic compounds can be produced from CO₂ immediately after a meteorite impact. (In future, we will carry out simulations adding nitrogen source molecules such as N₂ and NH₃ to the model.) During impact compression for several picoseconds in our shock wave simulations, we have observed formation of some C-H bonds, which was the basic element of hydrocarbons. The formation of C-H bonds occurred on the Fe surface, and it was found that the reaction processes have many similarities to the Fischer-Tropsch (FT) process as expected in the previous study. [7] In addition, the production of formic acid (HCOOH) which is the simplest carboxylic acid has been observed. It should be also noted particularly that HCO₃⁻ ions formed from CO₂ and H₂O molecules played an important role as intermediates for the production of both C-H bonds and a HCOOH. All the production processes above will be reported in detail using snapshots of the atomic configurations and population analysis. [16, 17] These results would provide novel insights into what reaction processes occurred and then resulted in production of the organic compounds at the meteorite impact on ocean.

2 | METHOD OF CALCULATION

Our calculation model consists of 16 CO₂ and 38 H₂O molecules, as well as an Fe₃₆ slab (a total of 198 atoms; see Fig. 1). The Fe₃₆ slab was initially prepared as 2 × 3 × 3 bcc unit cell. A rectangular supercell of dimensions 30.74 Å × 8.083 Å × 8.089 Å under a periodic boundary condition was employed. This system represents the initial reactions when an iron-bearing meteorite (the Fe₃₆ slab) collides with CO₂ dissolved in the sea. The amount of CO₂ is much higher than the dissolution amount assumed in the previous study (130 mM [18]). To investigate various reactions, we prepared such a model with high CO₂ concentration. Structural optimization by quasi-Newton method [19] was performed to prepare an initial atomic configuration. Using this atomic configuration, we performed two MSST-AIMD simulations, where shock waves propagated in the *x* direction with shock speeds of 5 and 4 km/s. It is worth noting that we have performed a short simulation (1 ps) under the same initial condition except shock waves, where only trivial reactions that two H₂O and one CO₂ were additionally physisorbed on the Fe slab surfaces were observed. This means that no reductive compounds are produced without shock waves in our model. We used our own AIMD code, [20] which has been implemented on parallel computers using the message passing interface library for interprocessor communications. In our simulations, electronic states were calculated using the projector-augmented-wave (PAW) method. [21, 22] Projector functions were generated for the 2*s* and 2*p* states of C and O atoms, the 1*s* state for H, and the 2*p*, 3*d*, 4*s*, and 4*p* states of Fe atoms. The generalized gradient approximation [23] was used for the exchange-correlation energy with non-linear core corrections. [24] Spin polarization effects were not included here. We employed the DFT-D method for the semi-empirical correction of the van der Waals interaction. [25] The momentum-space formalism [26] was utilized, where the plane wave cutoff energies were set to be 30 and 250 Ry for the electronic pseudo-wave functions and the pseudo-charge density, respectively. The Γ point was used for Brillouin zone sampling. The energy functional was minimized iteratively using a preconditioned conjugate-gradient method. [27, 28]

The MSST [12, 13] was utilized to simulate a stable planar shock wave, which modifies the atomistic equation of motion so that the volume of the simulation cell evolves over time while satisfying the Rayleigh line for stress and the Hugoniot relation for energy. [29] The dynamics of the system is governed by the following extended Lagrangian,

$$L = \frac{1}{2} \sum_i m_i (\mathbf{h}q_i)^t (\mathbf{h}q_i) - \Phi(\{\mathbf{h}q_i, \mathbf{h}\}) + \frac{Q}{2M} \dot{V}^2 + \frac{1}{2} M V_s^2 \left(1 - \frac{V}{V_0}\right)^2 - P_0(V - V_0), \quad (1)$$

where m_i is the mass of the i th atom, \mathbf{q}_i is a column vector whose components are the i th atom's scaled coordinates in the range of $[0, 1]$, Φ is the potential energy, Q is a parameter with unit of $(\text{mass})^2 \cdot (\text{length})^{-4}$, $M = \sum_i m_i$ is the total mass of the system, and V_s is the speed of the shock wave. The real coordinate and the velocity of the i th atom are given by $\mathbf{h}\mathbf{q}_i$ and $\mathbf{h}\dot{\mathbf{q}}_i$ respectively, where $\mathbf{h} = (\mathbf{L}_1 \ \mathbf{L}_2 \ \mathbf{L}_3)$ is a matrix consisting of the computational cell lattice vectors \mathbf{L}_k ($k = 1, 2$, and 3). $V = \det \mathbf{h}$ is the volume of the computational cell. P_0 and $V_0 = \det \mathbf{h}_0$ are the pressure and volume of the unshocked state, respectively, where \mathbf{h}_0 corresponds to \mathbf{h} in the unshocked state. In eq. (1), a dot denotes time derivative. Initial pressure and temperature for the two MSST-AIMD simulations were set to 0 GPa and 300 K, respectively. The equations of motion were integrated numerically with a time step Δt of 10 a.u. ($= 0.242$ fs). Note that one specifies the shock speed (V_s) in the MSST, and we set 5 and 4 km/s in this study. The MSST-AIMD simulations with $V_s = 5$ and 4 km/s were performed for the time durations of 7 and 5 ps, respectively.

Our simulation code has already been used successfully for shock MD simulations. [13, 30] The shock simulations for a molecular crystal of TriAminoTrinitroBenzene (TATB) which is known as one of the energy materials were consistent with the dynamics of quantum MD simulation performed by other research groups (Manaa *et al.* [31]). In addition to temporal changes of temperature and pressure, the products also matched as well.

To quantify the change in the bonding properties of atoms involved in production reactions of the organic compounds, we conducted a population analysis [16, 17] by expanding the electronic wave functions in an atomic-orbital basis set. [32, 33] Based on the formulation generalized to the PAW method, [34] we obtained the bond-overlap population (BOP or $O_{ij}(t)$) between i th and j th atoms and the gross population $Z_i(t)$ for i th atom. The Mulliken charge $Q_i(t)$ was then obtained as the difference between the number of valence electrons of an isolated neutral atom $Z_i^0(t)$ and the value of the gross population $Z_i(t)$:

$$Q_i(t) = Z_i^0(t) - Z_i(t). \quad (2)$$

We estimated the charges of the atoms from $Q_i(t)$. $O_{ij}(t)$ gives a semi-quantitative estimate of the strength of covalent bonds between atoms. Note that a bonding state exists between i th and j th atoms if O_{ij} shows a positive value. Conversely, an antibonding state exists if O_{ij} shows a negative value. The charge spillage estimating the expansion error [32] is about 0.4%, which indicates the high accuracy of the atomic-orbital basis set.

To calculate the numbers of interatomic bonds, a bond was defined between two atoms that were within the cutoff length continuously for a prescribed lifetime as in our previous studies. In this study, we investigated the H-O, H-C, H-Fe, C-O, C-Fe, and O-Fe bonds. For H-O bonds, O atoms are distinguished from those derived from H_2O (O_w) and from CO_2 (O_c). The lifetime was chosen to be 2.42 fs, and the cutoff lengths for H-O (both H- O_w and H- O_c), H-C, H-Fe, C-O, C-Fe, and O-Fe bonds were 1.25, 1.50, 2.40, 1.60, 2.40, and 2.40 Å, respectively. The cutoff lengths were determined from the first minima of partial radial distribution functions obtained from the 5 km/s shock-wave simulation.

3 | RESULTS AND DISCUSSION

3.1 | Time Evolution of Physical Quantities

In preparation for discussions in the later subsections, we shows here the time evolution of the four physical quantities, *i.e.*, volume ratios (V/V_0 : V_0 is the initial volume), pressures (P), particle velocities (U_p) and temperatures (T) in the 5 and 4 km/s shock-wave simulations in Fig. 2. Since the particle velocity is comparable to an impact velocity of the meteorite, it is an important physical quantity to discuss the validity of the simulations.

All four physical quantities changed rapidly from 0 ps to approximately 0.2 ps for both simulations following a

gradual change over time. For the 5 km/s simulation, the respective values of V/V_0 , P , U_p , and T reached to 0.65, 25.0 GPa, 1.75 km/s, and 1500 K at 5 ps. Even at 7 ps, these values have almost unchanged. For the 4 km/s simulation, the respective values of V/V_0 , P , U_p , and T reached to 0.74, 13.2 GPa, 1.02 km/s, and 1100 K at 5 ps, due to the smaller shock speed compared to the 5 km/s simulation. In this way, the primordial ocean surface immediately after the meteorite collided would have been placed under the high temperature and pressure due to compression by shock waves.

Meanwhile, the particle velocities of our simulations would be in a realistic impact velocity range. These are much slower than a typical meteorite's impact velocity (above 10 km/s). [35] However, the effects of aerobraking by the Earth's atmosphere [36] and of deceleration of breakup while passing through the atmosphere [37] affect the impact velocity on planetary surface. Considering these effects, even if the initial velocity before entering the atmosphere is 10 km/s or higher, the impact velocity on the planetary surface could be decelerated to about 1 km/s. [37] This value would be comparable to the present simulations.

Moreover, we dealt with water around the Fe atoms as liquid phase, despite the temperature in our simulations exceeding the boiling point of that. It is considered that the behaviors of meteorites at the ocean collision were categorized into what had generated the impact plumes near the sea level containing the evaporated seawater and meteorite contents [5] and what had advanced into the deep sea. [38] Our simulations corresponded to the latter case.

3.2 | Organic compounds produced by the shock waves in the simulations

As mentioned in section 1, our purpose is to clarify production processes of the Organic compounds from CO_2 and H_2O via reduction by metallic iron. Contrary to our initial expectations, no hydrocarbons were produced whereas the production of carboxylic acid was observed in our simulations. However, several adsorbates on the Fe surface observed during the simulations have made us expect the production of hydrocarbons. As Furukawa *et al.* stated, [7] hydrocarbon production by Fischer-Tropsch (FT) process was expected in oceanic collisions of meteorites. Note that a lot of previous studies have also considered that the FT process played an important role for the synthesis of biomolecules in the nebula and terrestrial environment of the solar system [39, 40, 41, 42, 43]. The FT process is a surface chemical reaction that converts CO and H_2 to hydrocarbon using transition metal catalysts such as iron and nickel, [40] where the production reaction begins after CO and H_2 adsorb onto the catalyst. [44] The H_2 immediately dissociates on the catalyst to become single H atoms. In the primary step in the production of any hydrocarbon, the hydrogenation of CO and subsequently production of CH_4 can occur on the catalyst, that is: [44]



Actually, in our simulations, we observed reactions in which large numbers of $^*\text{H}$ atoms and $^*\text{CO}$ molecules were brought to the iron surface. Here, * denotes an adsorption site on the Fe surface. Thus, $^*\text{H}$ and $^*\text{CO}$ indicates that a single H atom and a carbon monoxide molecule are adsorbed on the Fe surface, respectively.

Bond analysis helps us to grasp roughly the reactions that occurred during the simulation. How to define interatomic bonds was described at the end of section 2. Figure 3(a) shows time evolution of the numbers of interatomic bonds between H-O_w , H-O_c , and H-C in the 5 and 4 shock simulations. In addition, Figures 3(b)-(e) show the time evolution of numbers of $^*\text{H}$ atoms, $^*\text{CO}$ molecules, $^*\text{COO}$ fragments, and HCO_3^- ions for the 5 and 4 km/s simulations.

Firstly, we describe the formation process of $^*\text{H}$ atoms. During the rapid compression period from 0 to 0.2 ps, a

large number of H atoms were released from the H_2O molecules. Reflecting the magnitude of the shock speeds, the numbers of dissociated H atoms from O atoms in H_2O molecules in the 5 and 4 km/s simulations were 24 (7 ps) and 13 (5 ps), respectively (see Fig. 3(a)). As will be described later in subsection 3.4, an example of the release mechanism was that densification by impact compression promoted the sharing of H atoms between H_2O molecules, and then H_3O_2 clusters were formed and the H atoms were released. [45] The chemisorbed H_2O molecules also released $^*\text{H}$ atoms. Importantly, some of the H atoms were supplied on the Fe surface (i.e. $^*\text{H}$ atoms). The numbers of $^*\text{H}$ atoms are shown in Fig. 3(b), where 7 and 3 $^*\text{H}$ atoms existed after 1 ps in the 5 and 4 km/s simulations, respectively. Other formation mechanisms of $^*\text{H}$ atoms will be described in subsection 3.5.

On the other hand, $^*\text{CO}$ molecules were formed from chemisorption of CO_2 molecules onto the Fe surface (called $^*\text{COO}$ fragments), the numbers of which are shown in Figs. 3(c) and 3(d). Note that the $^*\text{COO}$ fragments frequently repeated becoming the $^*\text{COOH}$ fragments and returning to the $^*\text{COO}$ fragments by being weakly bonded with a H atom and releasing it. Here, the number of $^*\text{COO}$ fragments including the $^*\text{COOH}$ fragments was displayed in Figs. 3(d). In addition to those formed from single CO_2 molecule, reactions involving several CO_2 molecules and HCO_3^- ions were also observed. The formation mechanisms are described in subsections 3.3, 3.4, and 3.8. The pressure and temperature during shock compression period is much higher than those of the Fischer-Tropsch reaction range (~ 600 K, ~ 40 bar) [42, 44], as shown in Figs. 2(b) and 2(c). We observed the formation of C-H bonds in the 5 km/s simulation (Fig. 3(a)), but the number of bonds was two at maximum. Therefore, we consider that preparations such as supply of the materials necessary for the FT process (i.e. $^*\text{H}$ atoms and $^*\text{CO}$ molecules) mainly progressed during the shock compression period, and the actual hydrocarbon production occurred during the subsequent adiabatic expansion period, [46, 47] when pressure and temperature dropped. If we simulate the adiabatic expansion period continuously from the atomic configuration of the shock compression period, the FT process may provide hydrocarbons as expected by the previous study. [7] We plan to perform such a study in future.

Furthermore, we have observed the production of a HCOOH in the 5 km/s shock-wave simulation. In subsection 3.8, this production process will be discussed separately for the process of forming a $^*\text{COO}$ fragment and the subsequent production process of a HCOOH . Although $^*\text{COO}$ in our simulations were often generated from CO_2 molecules (see subsection 3.3), the former $^*\text{COO}$ production process occurred from HCO_3^- . A HCO_3^- ion bonded to a $^*\text{O}$ atom became a carbon tetraoxide (CO_4) temporarily, resulting in a $^*\text{COO}$ fragment by reduction of Fe atoms at 5.32 ps in the 5 km/s simulation shown in Fig. 3(e). This reaction is of great interest in that the $^*\text{COO}$ fragment was formed on the surface even after the Fe surface was oxidized. The latter HCOOH production process is also interesting for considering the condition leading to a HCOOH rather than the $^*\text{CO}$. Most of $^*\text{COO}$ fragments formed in our simulations became $^*\text{CO}$ molecules, but this reaction only resulted in a HCOOH .

Importantly, it was found that HCO_3^- ions formed from CO_2 and H_2O molecules acted as important intermediates in the formation of the $^*\text{H}$ atoms and $^*\text{CO}$ molecules as well as the HCOOH . It may have been an indispensable performer that mediated between the inert carbon and hydrogen sources (CO_2 and H_2O) on the early Earth and Organic compounds such as hydrocarbons and carboxylic acids. How the HCO_3^- ion contributed to these formation processes will be described in subsections 3.4 and 3.8.

Moreover, we consider that the primary driving force of such chemical reactions observed in our simulation was the high-pressure densification. As mentioned above, CO_2 and H_2O molecules were chemisorbed onto the Fe surfaces and then became carbon and hydrogen sources, which facilitated the hydrocarbon production process like the FT process on the Fe surfaces. In addition, HCO_3^- ions formed from CO_2 and H_2O molecules also worked as carbon sources, and protons (H^+) transferred between H_2O molecules also acted as hydrogen sources. The time evolution of pressures and the numbers of products in the simulations with shock speeds of 5 and 4 km/s shown in Figs. 2 and 3 are quantitative data showing that the reductive products increased with pressure and would support that the high-pressure densification

was the dominant driving force.

In the following subsections, the production process of each product will be explained in detail using snapshots and the population analysis results. Subsection 3.3 describes formation mechanism of $^*\text{CO}$ molecules. In subsection 3.4, the production processes of HCO_3^- ions are discussed. Subsections 3.5 describes the production reaction of $^*\text{H}$ atoms. In subsections 3.6 and 3.7, we describe the mechanism of C-H bond formation, where after $^*\text{CO}$ molecule is reduced to a $^*\text{C}$ atom, a C-H bond is formed. Finally, the production process of HCOOH is described in the subsection 3.8.

3.3 | Formation mechanisms of $^*\text{CO}$ molecules on Fe surface

Here, we describe the formation process of a $^*\text{CO}$ molecule on the Fe surface. The formation occurred 4 times for both the 5 and 4 km/s simulations as shown in Fig. 3(c), but the reaction speed in the 5 km/s simulation was faster. As explained below, this is because the formation process was different, and the $^*\text{CO}$ molecules were formed by two reaction pathways. (As will be described later, the reason for the reduction in the number of $^*\text{CO}$ molecules from 4 to 2 in the 5 km/s simulation as shown in Fig. 3(c) is that the $^*\text{CO}$ molecule released its O atoms and became $^*\text{C}$ atoms.)

First, we explain the most frequent pathway using an example that occurred in the 5 km/s shock-wave simulation shown in Fig. 4(a). The reaction proceeded as follows:



where $*$ denotes an adsorption site on the Fe surface. Figure 4(b) shows the time evolution of the bond-overlap populations $O_{ij}(t)$ for specified atoms using the Mulliken bond-overlap population analysis (see section 2).

At 0.085 ps, a CO_2 molecule consisting of C1, O1, and O2 was adsorbed on the Fe surface due to the rapid compression by the shock wave, resulting in a $^*\text{COO}$ fragment. C1 bonded to Fe1, and O2 bonded to Fe2 ($O_{\text{C1-Fe1}}(t)$ and $O_{\text{O2-Fe2}}(t)$ have finite positive values). In contrast, the bond strengths of $O_{\text{C1-O1}}(t)$ and $O_{\text{C1-O2}}(t)$ decreased. Subsequently, C1 also bonded to Fe3, and O1 bonded to Fe5 and Fe6 at 0.155 ps. Thus, the bond strength between C1-O1 was further decreased. At 0.210 ps, $O_{\text{C1-O1}}(t)$ finally vanished, i.e. O1 was dissociated from C1. This means that a $^*\text{CO}$ molecule consisting of C1 and O2 was formed. Such a $^*\text{CO}$ molecule formation occurred at 1 and 4 times for the 5 and 4 km/s simulations, respectively. All the $^*\text{CO}$ formed in the 4 km/s simulation was through the above reaction pathways. On the other hand, the formation of the remaining three $^*\text{CO}$ molecules in the 5 km/s shock-wave simulation occurred through the formation of HCO_3^- ions as described in the next subsection 3.4. The reason why the 5 km/s shock-wave simulation had a higher $^*\text{CO}$ formation rate is due to such existence of two formation mechanisms.

3.4 | Formation mechanisms of HCO_3^- ions

In this subsection, we describe the three mechanisms of HCO_3^- ion formation observed in our simulation. Along with these HCO_3^- ion formations, $^*\text{CO}$ molecules and $^*\text{H}$ atoms were formed on the Fe surface. Fig. 3(e) shows the numbers of formed HCO_3^- ions in the 5 and 4 km/s simulations, which rapidly increased with shock compression. An example of the first mechanism is shown in Fig. 5(a), where a CO_2 and two H_2O molecules were involved. The reaction proceeded

as follows:

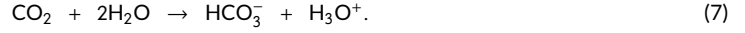


Figure 5(a) shows time evolution of the atomic configuration, where a HCO_3^- ion was formed at 0.250 ps. Figure 5(b) shows the time evolution of $O_{ij}(t)$ for specified pair atoms. The three molecules at 0.175 ps shown in Fig. 5(a) were close to each other by high pressure. At 0.205 ps, C1 bonded to O1 and the bond between H1 and O1 began to weaken (see $O_{\text{C1-O1}}(t)$ and $O_{\text{H1-O1}}(t)$). In addition, a proton transfer occurred by Grotthuss mechanism [48] due to H1 forming a bond with O2 of the nearby H_2O molecule. Subsequently, the strength of H1-O1 bond vanished, *i.e.*, a HCO_3^- ion and a H_3O^+ ion were formed at 0.250 ps. The dissociated protons (H^+ or H_3O^+) were transferred between surrounding H_2O molecules, and some of them resulted in $^*\text{H}$ atoms on the Fe surface. See subsection 3.5 for details of the formation reaction of $^*\text{H}$ atoms.

The formation of HCO_3^- ion by the second mechanism occurred near the Fe surface. Figure 5(c) shows an example occurring in the 5 km/s shock-wave simulation. The reaction proceeded as follows:

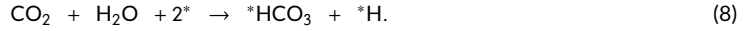


Figure 5(c) shows time evolution of the atomic configuration, where a HCO_3^- ion was formed at 0.070 ps. Figure 5(d) shows the time evolution of $O_{ij}(t)$ for specified pair atoms. CO_2 and H_2O molecules were involved in this mechanism. The corresponding reaction was observed only once before 0.2 ps in both 5 and 4 km/s simulations. At 0.035 ps, the CO_2 and H_2O molecules were pressed down on the Fe surface, and then two bonds of O3-Fe1 and H2-Fe2 were formed ($O_{\text{O3-Fe1}}(t)$ and $O_{\text{H2-Fe2}}(t)$ have finite positive values for $t > 0.035$ ps). Conversely, the bond strengths between C2-O3 and H2-O4 ($O_{\text{C2-O3}}(t)$ and $O_{\text{H2-O4}}(t)$) decreased. Since C2 therefore had one more electron not used for bonding, C2 newly formed a bond with O4 ($O_{\text{C2-O4}}(t)$) at 0.070 ps. Then, H2 was released from O4 to the Fe surface, *i.e.*, one HCO_3^- ion was produced. (However, it is noted, strictly, that this was not a HCO_3^- ion but a $^*\text{HCO}_3$ due to the remaining bond between O3 and Fe1.) The dissociated H2 moved around the Fe surface while making and cutting bonds with many Fe atoms. H2 bonded to Fe2 and Fe3 at 0.070 ps, but bonded to Fe1 at 0.150 ps. This second mechanism is important in that H atoms were supplied directly to the Fe surface.

The HCO_3^- ion formation by the third mechanism also occurred near the Fe surface. An example that occurred in the 5 km/s shock-wave simulation is shown in Fig. 5(e), where a CO_2 molecule, a $^*\text{COO}$ fragment, and a H_3O^+ ion were involved. The reaction proceeded as follows:



Figure 5(e) shows time evolution of the atomic configuration, where a HCO_3^- ion was formed at 0.335 ps. Figure 5(f) shows the time evolution of $O_{ij}(t)$ for specified pair atoms. The $^*\text{COO}$ fragment and H_3O^+ ion on the left hand of eq.(9) were mainly formed through the reactions eq.(5) and eq.(7), respectively. Particularly, it is important that a $^*\text{CO}$ molecule was formed in this mechanism. At around 0.200 ps, H3 of H_3O^+ ion bonded to O5 ($O_{\text{H3-O5}}(t)$ had 0.7), and then a $^*\text{COOH}$ fragment was formed. A CO_2 molecule present near the $^*\text{COOH}$ fragment formed a bond of C4-O5 at 0.280 ps (see $O_{\text{C4-O5}}(t)$ in Fig. 5(f)). Because of transfer of a OH^- ion consisting of H3 and O5 to the CO_2 molecule, one HCO_3^- ion and one $^*\text{CO}$ molecule were formed on the Fe surface at 0.335 ps. Although this third mechanism could not be observed in the 4 km/s simulation,

it was realized three times in the 5 km/s one. The reason why the formation rate of $^*\text{CO}$ molecules in the 5 km/s simulation exceeded that in the 4 km/s one (see Fig. 3(c)) is considered to be due to that this pathway is present in addition to the pathway of eq.(7). In order for this third mechanism to take place, it would be necessary that the associated atoms are close enough to form bonds, that is, compressibility would be an important factor.

3.5 | Formation mechanisms of single $^*\text{H}$ atoms on Fe surface

In addition to being formed together with HCO_3^- ion (i.e. eq.(8)), single $^*\text{H}$ atoms on the Fe surface were also formed by the following three mechanisms. With a high pressure, molecules are more strongly pressed toward the Fe surface, so there was a distinct difference in the numbers of $^*\text{H}$ atoms between the 5 and 4 km/s simulations as shown in Fig. 2(b).

First, a $^*\text{H}$ atom was directly supplied by a H_3O^+ ion. The reaction proceeded as follows:



Figure 6(a) shows time evolution of the atomic configuration in an example reaction process by the first mechanism, where a $^*\text{H}$ atom (H1) was formed at 0.045 ps. Figure 6(b) shows the time evolution of $O_{ij}(t)$ for specified pair atoms. In Fig. 6(a), H1 of a H_3O^+ ion formed a bond with Fe1 ($O_{\text{H1-Fe1}}(t)$ increased for $t > 0$ ps). Afterwards, $O_{\text{H1-Fe1}}(t)$ was decreased to zero at 0.045 ps, that is, a $^*\text{H}$ atom (H1) was formed. Such a production reaction occurred three times and once in the 5 and 4 km/s simulations, respectively.

Second, a $^*\text{H}$ atom was supplied due to dissociation of a H_2O molecule adsorbed on the Fe surface:



Figure 6(c) shows time evolution of the atomic configuration in an example reaction process by the second mechanism, where a $^*\text{H}$ atom (H2) was formed at 1.040 ps. Figure 6(d) shows the time evolution of $O_{ij}(t)$ for specified pair atoms. At 0.970 ps, H2 of the adsorbed H_2O molecule on Fe2 formed a weak bond with Fe3 ($O_{\text{H2-Fe3}}(t) < 0.25$). Simultaneously, O2 also formed a bond with Fe3 (see $O_{\text{O2-Fe3}}(t)$). The formation of these bonds caused weakening the H2-O2 bond. While the H2-Fe3 bond was completely broken at 1.015 ps, H2 formed a strong bond to Fe4 instead ($O_{\text{H2-Fe4}}(t) > 0.25$). Finally, the strength of H2-O2 bond vanished at 1.040 ps, and then a $^*\text{H}$ atom (H2) was formed. Such a production reaction took place twice only in the 5 km/s simulation.

Third, a $^*\text{H}$ atom was supplied to the iron surface by a H_3O^+ ion and a HCO_3^- ion, which occurred once in the 5 km/s simulation. The reaction proceeded as follows:

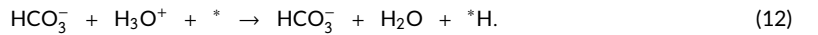


Figure 6(e) shows time evolution of the atomic configuration in an example reaction process by the third mechanism, where a $^*\text{H}$ atom (H3) was formed at 1.700 ps. Figure 6(f) show the time evolution of $O_{ij}(t)$ for specified pair atoms. At around 1.670 ps, H3 of the HCO_3^- ion bonded to Fe5 and Fe6, with being accompanied by forming a bond between O3 and H4 of a H_3O^+ ion ($O_{ij}(t)$ for H3-Fe5, H3-Fe6, and H4-O3 increased for $t > 1.670$ ps). As a result, the bond between O3 and H3 became unstable, and then H3 strengthened the

interactions with Fe5 and Fe6. Since proton transfers occurred at 1.700 ps, H4 moved to O3 and then H3 was released to the Fe surface, *i.e.*, a *H atom (H3) was formed.

3.6 | Formation mechanisms of single *C atoms on Fe surface

It is believed that a *CO molecule releases its O atom in a form of H₂O molecule by being supplied with two H atoms and then becomes a single *C atom in the FT process. [44] Like the FT process, the formation of *C atom from *CO molecule was observed twice in the 5 km/s simulation. These occurred in the following hydrogenation processes:



An example of the formation process is shown in Fig. 7(a). Figure 7(b) shows the time evolution of $O_{ij}(t)$ for specified pair atoms. At 4.00 ps, a *CO molecule consisting of C1 and O1 existed on the Fe surface. When two H₃O⁺ ions approached to the *CO molecule at 4.17 ps, their H1 and H2 were bonded to O1 of the *CO molecule ($O_{H1-O1}(t)$ and $O_{H2-O1}(t)$ increased for $t > 4.10$ ps). Along with the formation of these bonds, the bond strength of C1-O1 ($O_{C1-O1}(t)$) started to decrease and then reached zero at around 4.48 ps. As the result, a H₂O molecule consisting of O1, H1, and H2 were released, leaving a single *C atom (C1). Such reactions would occur in the system where there were excessive H⁺ (H₃O⁺) ions in the surroundings of Fe surface like in the 5 km/s simulation.

3.7 | Formation mechanisms of C-H bonds on Fe surface

When single *C atoms appeared on the Fe surface, a stable C-H bond was finally formed. This reaction proceeded as follows:



An example of time evolution of the atomic configuration is shown in Fig. 7(c). Figure 7(d) shows the time evolution of $O_{ij}(t)$ for specified pair atoms. While a H atom was supplied to the Fe surface in the reaction of eq.(10), a H atom was supplied to the *C atom in the reaction of eq.(15). This is because the single *C atom had a negative charge similar to the O atoms of H₂O molecules and it was chosen as a destination of proton transfers which have been carried out between H₂O molecules. Figure S1 in supplementary material (SM) shows time evolution of Mulliken charge of C1 (Q_{C1}) and the average charge of O atoms of H₂O molecules. Although Q_{C1} was neutral at 0 ps due to the CO₂ state, the charge value reached -0.90 at around 4.5 ps, when C1 became a *C atom. This value is consistent with the average Mulliken charge of O atoms of H₂O molecules ~ -0.9 . Such a formation of C-H bond via proton transfer rapidly occurred. Since H₂O molecules are not used as materials in the actual FT process, the *H atoms on the Fe surface would diffuse and bond to the *C atoms. [44] In our simulation, there is a possibility that the C-H bonds were formed by two H atom supply mechanisms of proton transfers between H₂O molecules as well as their diffusion on the Fe surface. Actually,

the C-H bond formation due to diffusion of $^*\text{H}$ atoms actually occurred during formation of HCOOH described in the next subsection 3.8.

Meanwhile, in the state of a $^*\text{CO}$ molecule, the formation of a stable C-H bond may be difficult, although it is considered to be a possible pathway in the previous study. [44] Figure S2 in SM shows an example in which a C-H bond was formed temporarily. The short-lived bond would have been broken not only by steric hindrance but also due to that the C atom did not have sufficient electrons. In fact, the Mulliken charge of C atom of the $^*\text{CO}$ molecule had only -0.5, which was about half charge of $^*\text{C}$ atom -0.9 (see Fig. S1 in SM).

3.8 | Production mechanism of a HCOOH

Finally, the formation process of HCOOH is described here. It was observed once in the 5 km/s simulation. Briefly, $^*\text{COO}$ fragment (strictly, $^*\text{COOH}$ fragment) was formed from a HCO_3^- ion as a reactant, and then a $^*\text{H}$ atom diffusing on the Fe surface was bonded to the $^*\text{COOH}$ fragment to form a HCOOH .

First, as shown in Fig. 8(a), one HCO_3^- ion was bonded to the $^*\text{O}$ atom (O1) on the Fe surface to form a carbon tetraoxide (CO_4) at 3.75 ps:

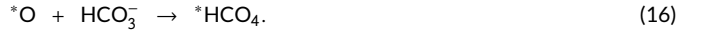
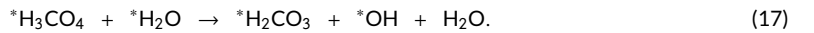


Figure 8(b) shows the time evolution of $O_{ij}(t)$ for specified pair atoms. More strictly, several H atoms were bonded to the O atoms, but their bonding states greatly varied with time. We therefore call it carbon tetraoxide for convenience. The H atoms participating in the focused reaction are made visible in Fig. 8(a). The carbon tetraoxide was never produced in the 4 km/s simulation, while two tetraoxides were formed in the 5 km/s simulation at 0.88 and 3.75 ps. However, the former tetraoxide was returned to a HCO_3^- ion and $^*\text{O}$ atom at 2.65 ps. In addition, O1 was formed by dissociating a H atom from the state of a $^*\text{OH}$ fragment as seen in eq.(11) (or see Fig. 6(d)).

At 4.50 ps, C1 of the carbon tetraoxide dissociated one O atom (O4) to produce a H_2O molecule as shown in Fig. 8(c), and then instead bonded to Fe1 at 4.67 ps:



This reaction from 4.50 to 4.67 ps would be a nucleophilic substitution reaction known as an SN_2 reaction in which a H_2O molecule and Fe1 corresponded to a leaving group and a nucleophilic agent, respectively.

As shown in Fig. 8(e), after H2 was also dissociated at 4.85 ps, O1 started to strengthen the bond with C1 at around 5.27 ps (see $O_{\text{C1-O1}}(t)$ in Fig. 8(f)). Conversely, the strength between C1-O3 bond ($O_{\text{C1-O3}}(t)$) rapidly weakened for dissociation at 5.32 ps, *i.e.*, O3 was dissociated from C1. This reaction formed a $^*\text{COOH}$, that is:



Thereafter, as shown in Fig. 8(g), a H^* atom diffusing on the Fe surface (H3) formed a bond with C1, accompanied with gradually weakening the bond between C1-Fe1. Finally, a HCOOH was produced at 6.75 ps:



It is emphasized that the $^*\text{COOH}$ fragment (or $^*\text{COO}$ fragment) in Fig. 8(e) was already seen in Fig. 4(a) or Fig. 5(e) as a precursor of $^*\text{CO}$ molecule. Therefore, there was a possibility of forming not only HCOOH but also $^*\text{CO}$ from $^*\text{COOH}$. Here, the HCOOH was formed because there were a lot of $^*\text{H}$ atoms on the Fe surface in the 5 km/s simulation as shown in Fig. 2(b). It would be difficult to produce a HCOOH at the beginning of the simulation because few H atoms were present on the Fe surface.

Furthermore, the SN_2 reaction of carbon tetraoxides formed from a HCO_3^- ion could provide $^*\text{COOH}$ even on the Fe surface oxidized by O atoms. However, since a carbon tetraoxide was not formed in the 4 km/s simulation, high pressure condition would be necessary. Conversely, if shock-wave simulation with higher shock speed (for example 6 km/s or more) is performed, more carbon tetraoxides will be formed and it is possible to form $^*\text{COOH}$ (or $^*\text{COO}$) on the Fe surface.

It is noted that the HCOOH produced at 6.75 ps bonded to the Fe surface again at 6.80 ps and then released its H atom to return to a $^*\text{COOH}$ fragment. Probably formation and collapse may be repeated under such a high pressure environment. Therefore, we think that it is important to investigate what will happen in simulations such as those for adiabatic expansion process [46, 47] in the future.

4 | CONCLUSION

By means of *ab initio* molecular dynamics combined with multi-scale shock technique (MSST-AIMD), we have investigated the possible prebiotic production processes of Organic compounds from CO_2 and H_2O by the reduction effect of metallic iron during the shock compression of meteorite impacts on ocean. By examining the reactions that occurred in the simulations in detail, we have found that the situation on the Fe surface was similar to the FT process, where $^*\text{CO}$ molecules and $^*\text{H}$ atoms were supplied and formed C-H bonds while diffusing on Fe surface. Although no hydrocarbon itself has been observed within our calculation time, the production may proceed in a reaction close to the FT process if we perform longer calculations in the future. In addition, we also observed the production of HCOOH that is the simplest carboxylic acid. The important finding is that HCO_3^- was involved in almost all of the productions of $^*\text{CO}$ molecules, $^*\text{H}$ atoms, and a HCOOH . It was found that $^*\text{H}$ atoms and $^*\text{CO}$ molecules were supplied on Fe surface when a HCO_3^- ion was formed and HCO_3^- also became the starting material for HCOOH production. Therefore it is possible that the formation process of HCO_3^- itself may have played an important role in the preparation of prebiotic production of Organic compounds at the events of meteorite impacts on ocean.

Besides simulations with higher shock speeds or with longer duration, we intend to run them under a variety of other different initial conditions. We used excessive CO_2 concentration in this study to find as many chemical reactions as possible within limited simulation time, but need to try simulations with more realistic concentrations. For the Fe atomistic configuration, the slab structure in this study is only one possibility and there may be other structures such as clusters. In addition, the actual sea water contains various kinds of ions such as Na^+ , Mg^{2+} , and Cl^- , so it would be necessary to investigate their influence on Fe surfaces. However, to comprehensively attempt such possibilities, the calculation cost of MD simulation based on DFT would be too large. We will thus focus on MSST-MD simulation method based on Density Functional Tight-Binding (DFTB) like Goldman *et al.* performed. [46, 47] This method approximates DFT by introducing several fitting parameters, and instead enables us to enlarge the MD simulation model and to accelerate its calculation. However, it is necessary to carefully validate the obtained results, and we are currently conducting its tests.

ACKNOWLEDGEMENTS

The financial supports of KAKENHI (16K17782, 17H06353, 18K03825, and 26460035) are gratefully acknowledged. This research used in part computational resources of HPCI-JHPCN System Research Project (Project ID: hp160056, hp160057, and jh170058-NAHI). The authors also kindly acknowledge the Supercomputer Center, Institute for Solid State Physics, The University of Tokyo, for the use of its facilities.

ENDNOTES

REFERENCES

- [1] Kasting JF. Earth's Early Atmosphere. *Science* 1993;259(5097):920–926.
- [2] Zahnle K, Schaefer L, Fegley B. Earth's Earliest Atmospheres. *Cold Spring Harb Perspect Biol* 2010;2(10):a004895.
- [3] Rosing M. C-13-Depleted Carbon Microparticles in > 3700-Ma Sea-Floor Sedimentary Rocks from West Greenland. *Science* 1999;283(5402):674–676.
- [4] Hassenkam T, Andersson MP, Dalby KN, Mackenzie DMA, Rosing MT. Elements of Eoarchean Life Trapped in Mineral Inclusions. *Nature* 2017;548:78–81.
- [5] Nakazawa H, Sekine T, Kakegawa T, Nakazawa S. High Yield Shock Synthesis of Ammonia from Iron, Water and Nitrogen Available on the Early Earth. *Earth Planet Sci Lett* 2005;235(1-2):356–360.
- [6] Furukawa Y, Sekine T, Oba M, Kakegawa T, Nakazawa H. Biomolecule Formation by Oceanic Impacts on Early Earth. *Nat Geosci* 2009;2(1):62–66.
- [7] Furukawa Y, Samejima T, Nakazawa H, Kakegawa T. Experimental Investigation of Reduced Volatile Formation by High-temperature Interactions among Meteorite Constituent Materials, Water, and Nitrogen. *Icarus* 2014;231:77–82.
- [8] Furukawa Y, Nakazawa H, Sekine T, Kobayashi T, Kakegawa T. Nucleobase and Amino Acid Formation through Impacts of Meteorites on the Early Ocean. *Earth Planet Sci Lett* 2015;429:216–222.
- [9] Schoenberg R, Kamber B, Collerson K, Moorbath S. Tungsten Isotope Evidence from Similar to 3.8-Gyr Metamorphosed Sediments for Early Meteorite Bombardment of the Earth. *Nature* 2002;418(6896):403–405.
- [10] Gomes R, Levison H, Tsiganis K, Morbidelli A. Origin of the Cataclysmic Late Heavy Bombardment Period of the Terrestrial Planets. *Nature* 2005;435(7041):466–469.
- [11] Bottke WF, Vokrouhlicky D, Minton D, Nesvorny D, Morbidelli A, Brasser R, et al. An Archaean Heavy Bombardment from a Destabilized Extension of the Asteroid Belt. *Nature* 2012;485(7396):78–81.
- [12] Reed EJ, Fried LE, Joannopoulos JD. A Method for Tractable Dynamical Studies of Single and Double Shock Compression. *Phys Rev Lett* 2003;90:235503.
- [13] Shimamura K, Misawa M, Ohmura S, Shimojo F, Kalia RK, Nakano A, et al. Crystalline Anisotropy of Shock-Induced Phenomena: Omni-Directional Multiscale Shock Technique. *Appl Phys Lett* 2016;108(7):071901.
- [14] Shimamura K, Shimojo F, Nakano A, Tanaka S. Meteorite Impact-Induced Rapid NH₃ Production on Early Earth: *Ab Initio* Molecular Dynamics Simulation. *Sci Rep* 2016;6:38953.
- [15] Shimamura K, Shimojo F, Nakano A, Tanaka S. Meteorite Impacts on Ancient Oceans Opened up Multiple NH₃ Production Pathways. *Phys Chem Chem Phys* 2017;19:11655–11667.

- [16] Mulliken RS. Electronic Population Analysis on LCAO-MO Molecular Wave Functions. I. J Chem Phys 1955;23(10):1833–1840.
- [17] Mulliken RS. Electronic Population Analysis on LCAO-MO Molecular Wave Functions. II. Overlap Populations, Bond Orders, and Covalent Bond Energies. J Chem Phys 1955;23(10):1841–1846.
- [18] Aubrey AD, Cleaves HJ, Bada JL. The Role of Submarine Hydrothermal Systems in the Synthesis of Amino Acids. Orig Life Evol Biosph 2009;39(2):91–108.
- [19] Head JD, Zerner MC. A Broyden-Fletcher-Goldfarb-Shanno optimization procedure for molecular geometries. Chem Phys Lett 1985;122(3):264–270.
- [20] Shimojo F, Kalia RK, Nakano A, Vashishta P. Linear-Scaling Density-Functional-Theory Calculations of Electronic Structure Based on Real-Space Grids: Design, Analysis, and Scalability Test of Parallel Algorithms. Comput Phys Commun 2001;140(3):303–314.
- [21] Blöchl PE. Projector Augmented-Wave Method. Phys Rev B 1994;50(24):17953–17979.
- [22] Kresse G, Joubert D. From Ultrasoft Pseudopotentials to the Projector Augmented-Wave Method. Phys Rev B 1999;59(3):1758–1775.
- [23] Perdew JP, Burke K, Ernzerhof M. Generalized Gradient Approximation Made Simple. Phys Rev Lett 1996;77(18):3865–3868.
- [24] Louie SG, Froyen S, Cohen ML. Nonlinear Ionic Pseudopotentials in Spin-Density-Functional Calculations. Phys Rev B 1982;26(4):1738–1742.
- [25] Grimme S. Semiempirical GGA-type density functional constructed with a long-range dispersion correction. J Comp Chem 2006;27(15):1787–1799.
- [26] Ihm J, Zunger A, Cohen ML. Momentum-Space Formalism for the Total Energy of Solids. J Phys C 1979;12(21):4409.
- [27] Kresse G, Hafner J. *Ab Initio* Molecular-Dynamics Simulation of the Liquid-Metal-Amorphous-Semiconductor Transition in Germanium. Phys Rev B 1994;49(20):14251–14269.
- [28] Shimojo F, Kalia RK, Nakano A, Vashishta P. Linear-Scaling Density-Functional-Theory Calculations of Electronic Structure Based on Real-Space Grids: Design, Analysis, and Scalability Test of Parallel Algorithms. Comput Phys Commun 2001;140(3):303–314.
- [29] Reed EJ, Fried LE, Henshaw WD, Tarver CM. Analysis of Simulation Technique for Steady Shock Waves in Materials with Analytical Equations of State. Phys Rev E 2006;74:056706.
- [30] Shimamura K, Misawa M, Li Y, Kalia RK, Nakano A, Shimojo F, et al. A Crossover in Anisotropic Nanomechanochemistry of van der Waals Crystals. Appl Phys Lett 2015;107(23):231903.
- [31] Manaa MR, Reed EJ, Fried LE, Goldman N. Nitrogen-Rich Heterocycles as Reactivity Retardants in Shocked Insensitive Explosives. J Amer Chem Soc 2009;131(15):5483–5487.
- [32] Daniel SP, Emilio A, José MS. Analysis of Atomic Orbital Basis Sets from the Projection of Plane-Wave Results. J Phys Condens Matter 1996;8(21):3859–3880.
- [33] Segall MD, Shah R, Pickard CJ, Payne MC. Population Analysis of Plane-Wave Electronic Structure Calculations of Bulk Materials. Phys Rev B 1996;54(23):16317–16320.
- [34] Shimojo F, Nakano A, Kalia RK, Vashishta P. Electronic Processes in Fast Thermite Chemical Reactions: A First-Principles Molecular Dynamics Study. Phys Rev E 2008;77(6):066103.

- [35] Hughes DW, Williams IP. The Velocity Distributions of Periodic Comets and Stream Meteoroids. *Mon Not R Astron Soc* 2000;315(3):629–634.
- [36] Anders E. Pre-biotic Organic Matter from Comets and Asteroids. *Nature* 1989;342:255–257.
- [37] Baldwin B, Sheaffer Y. Ablation and Breakup of Large Meteoroids during Atmospheric Entry. *J Geophy Res* 1971;76(19):4653–4668.
- [38] Gersonde R, Deutsch A, Ivanov BA, Kyte FT. Oceanic Impacts - A Growing Field of Fundamental Geoscience. *Deep Sea Res Part 2 Top Stud Oceanogr* 2002;49(6):951 – 957.
- [39] Lewis J, Prinn R. Kinetic Inhibition of CO and N₂ Reduction in Solar Nebula. *Astrophys J* 1980;238(1):357–364.
- [40] Kress M, Tielens A. The role of Fischer-Tropsch catalysis in solar nebula chemistry. *Meteorit Planet Sci* 2001;36(1):75–91.
- [41] Hayatsu R, Anders E. Organic-Compounds in Meteorites And Their Origins. *Top Curr Chem* 1981;99:1–37.
- [42] Sekine Y, Sugita S, Kadono T, Matsui T. Methane Production by Large Iron Meteorite Impacts on Early Earth. *J Geophys Res-Planet* 2003;108(E7):5070.
- [43] Sekine Y, Sugita S, Shido T, Yamamoto T, Iwasawa Y, Kadono T, et al. An experimental study on Fischer-Tropsch catalysis: Implications for Impact Phenomena and Nebular Chemistry. *Meteorit Planet Sci* 2006;41(5):715–729.
- [44] Corral Valero M, Raybaud P. Cobalt Catalyzed Fischer-Tropsch Synthesis: Perspectives Opened by First Principles Calculations. *Catal Lett* 2013;143(1):1–17.
- [45] Vedadi MH, Haas S. Mechano-Chemical Pathways to H₂O and CO₂ Splitting. *Appl Phys Lett* 2011;99(15):154105.
- [46] Goldman N, Reed EJ, Fried LE, Kuo IFW, Maiti A. Synthesis of Glycine-Containing Complexes in Impacts of Comets on Early Earth. *Nat Chem* 2010;2(11):949–954.
- [47] Goldman N, Tamblyn I. Prebiotic Chemistry within a Simple Impacting Icy Mixture. *J Phys Chem A* 2013;117(24):5124–5131.
- [48] Shimamura K, Shimojo F, Kalia RK, Nakano A, Nomura KI, Vashishta P. Hydrogen-on-Demand Using Metallic Alloy Nanoparticles in Water. *Nano Lett* 2014;14(7):4090–4096.

5 | GRAPHICS

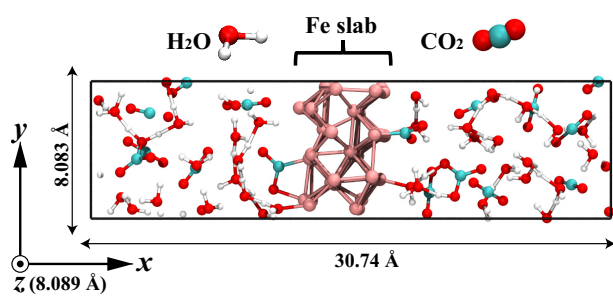


FIGURE 1 Initial atomic configuration of the system consisting of a Fe₃₆ slab, 16CO₂, and 38 H₂O molecules for the 5 and 4 km/s shock-wave simulations.

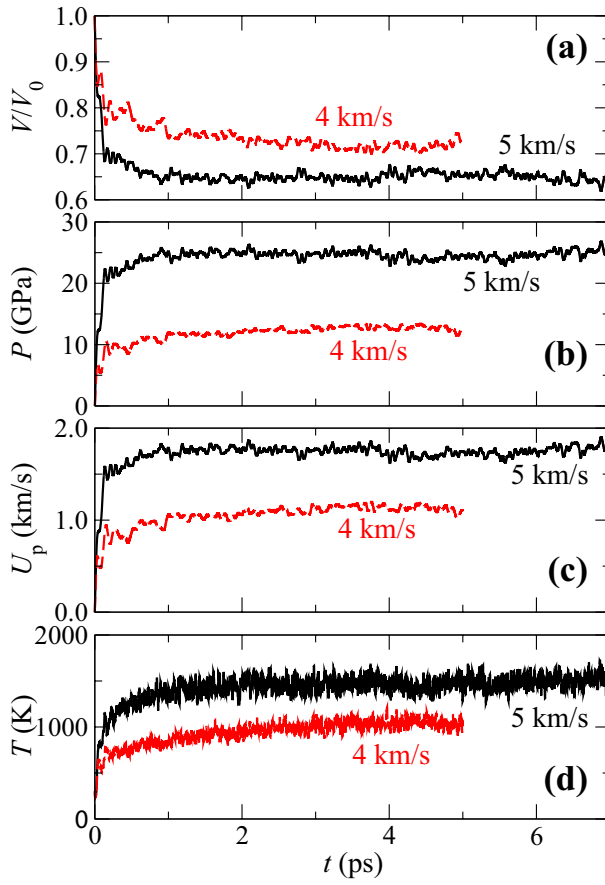


FIGURE 2 Time evolution of (a) volume ratios, (b) pressures, (c) particle velocities, and (d) temperatures in the 5 and 4 km/s shock-wave simulations.

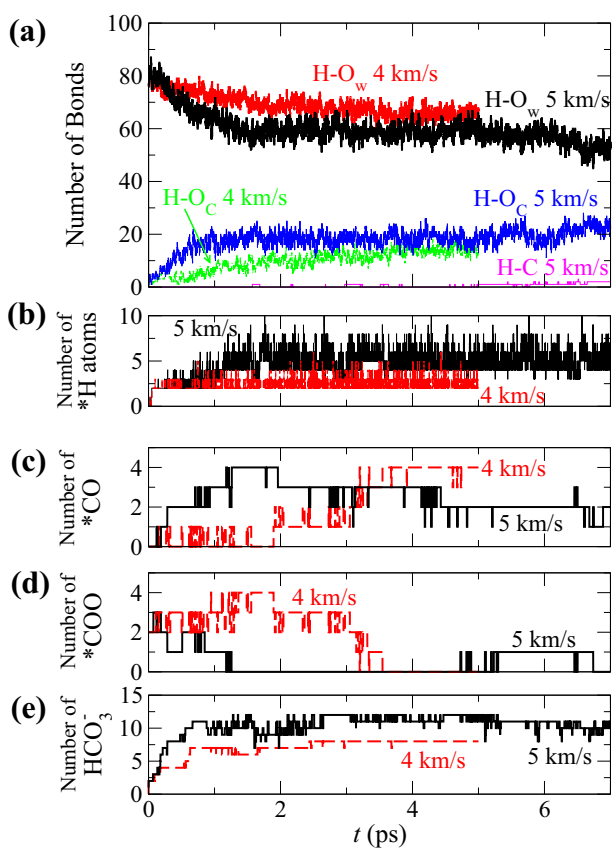


FIGURE 3 (a) Time evolution of the number of H-O_w , H-O_c , and H-C bonds in the 5 and 4 km/s shock-wave simulations, where O_w and O_c corresponds to the O atoms derived from H_2O and from CO_2 , respectively. Time evolution of the numbers of (b) *H atoms, (c) *CO molecules, (d) *COO fragments (including *COOH fragments), and (e) HCO_3^- ions in the 5 and 4 km/s shock-wave simulations.

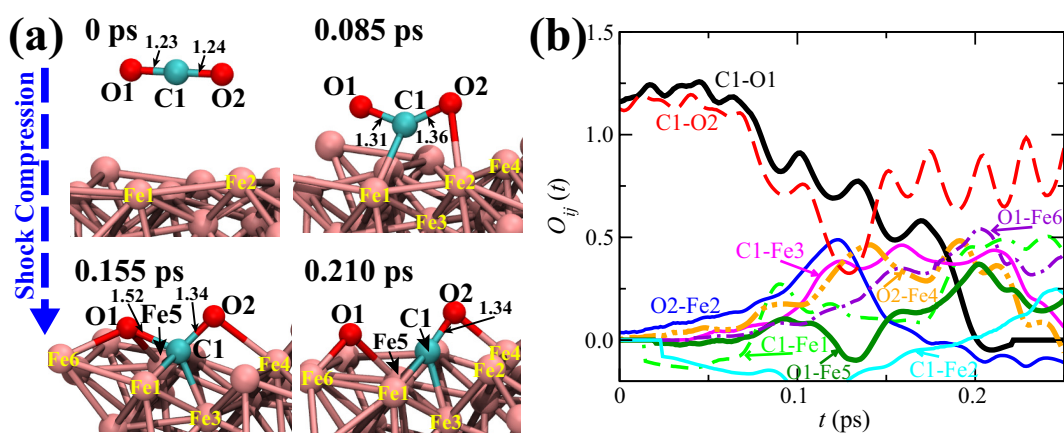


FIGURE 4 (a) Atomistic configurations during the formation of a $^*\text{CO}$ molecule on the Fe surface observed in the 5 km/s shock-wave simulation. Only the atoms participating in the reaction are visualized here. The real numbers indicate the distances of the selected bonds. The unit is Å. (b) Time evolution of the bond-overlap populations $O_{ij}(t)$ associated with the atoms labeled in (a).

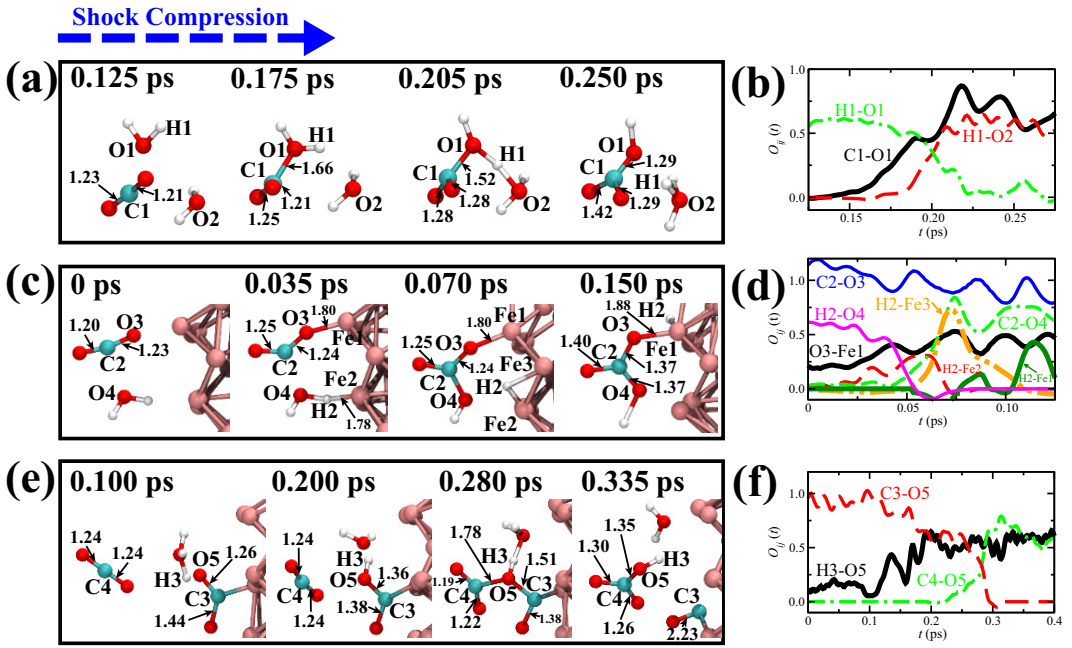


FIGURE 5 Atomistic configurations during the formation processes of a HCO_3^- ion by (a) the first, (c) second, and (e) third mechanisms (see text) observed in the 5 km/s shock-wave simulation, and time evolution of the corresponding bond-overlap populations $O_{ij}(t)$ ((b), (d), and (f)). Only the atoms participating in the reactions are visualized here. The real numbers shown in (a), (c), and (e) indicate the distances of the selected bonds. The unit is Å.

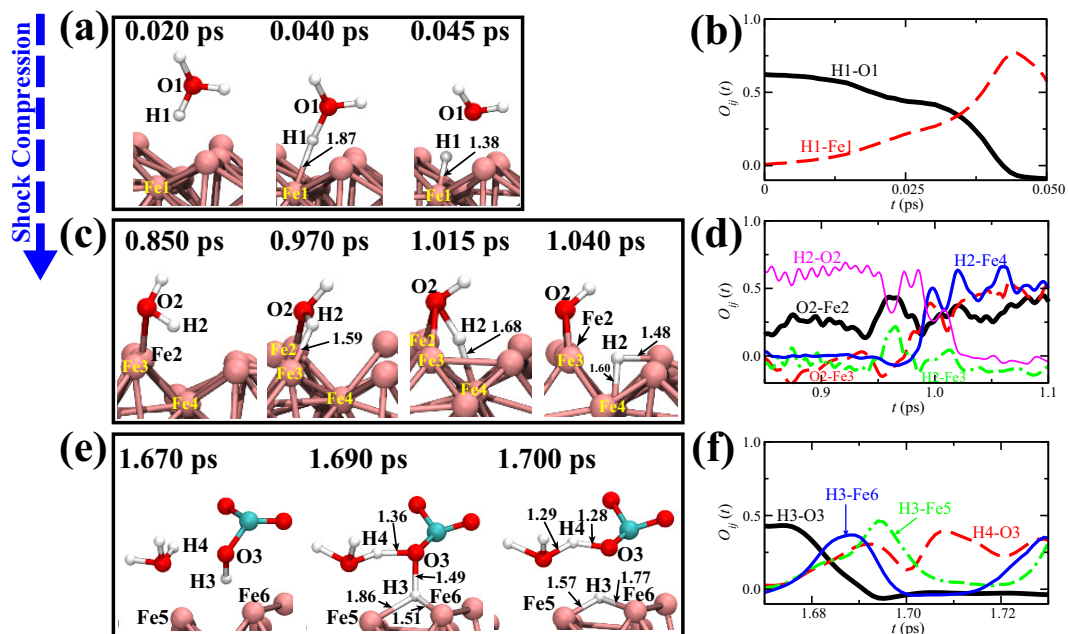


FIGURE 6 Atomistic configurations during the formation processes of a ${}^{\ast}\text{H}$ atom by (a) the first, (c) second, and (e) third mechanisms (see text) observed in the 5 km/s shock-wave simulation, and time evolution of the corresponding bond-overlap populations $O_{ij}(t)$ ((b), (d), and (f)). Only the atoms participating in the reactions are visualized here. The real numbers shown in (a), (c), and (e) indicate the distances of the selected bonds. The unit is Å.

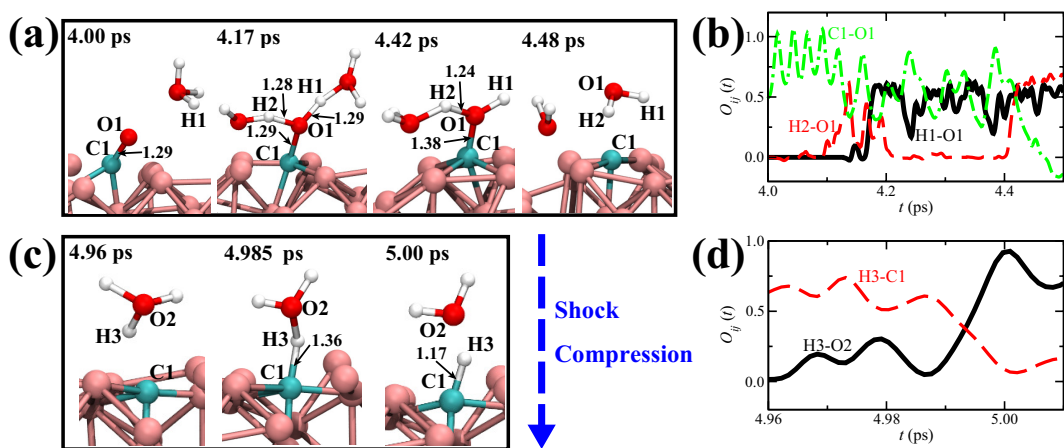


FIGURE 7 Atomistic configurations during the formation of (a) a ${}^*\text{C}$ atom from a ${}^*\text{CO}$ molecule and (c) the subsequent C-H bond formation observed in the 5 km/s shock-wave simulation. Time evolution of the corresponding bond-overlap populations $O_{ij}(t)$ are shown in (b) and (d). Only the atoms participating in the reactions are visualized here. The real numbers shown in (a) and (c) indicate the distances of the selected bonds. The unit is Å.

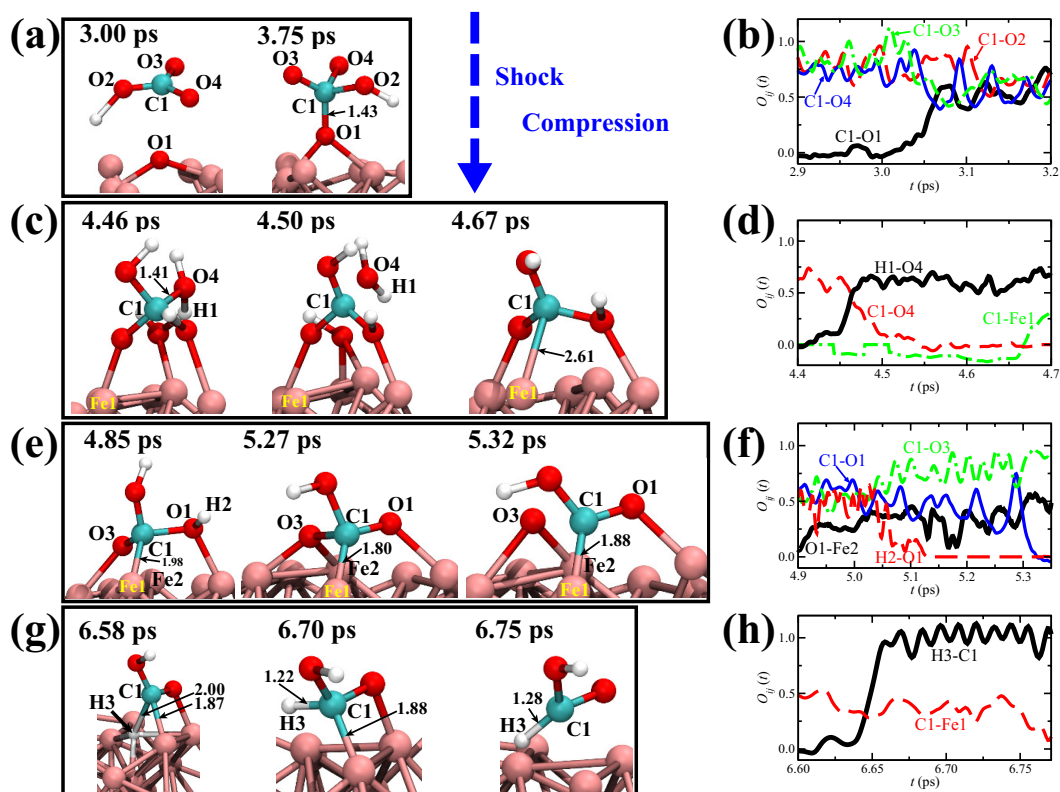


FIGURE 8 (a) Atomistic configurations during the production of a HCOOH observed in the 5 km/s shock-wave simulation ((a), (c), (e), and (g)). Time evolution of the corresponding bond-overlap populations $O_{ij}(t)$ are shown in (b), (d), (f), and (h). Only the atoms participating in the reactions are visualized here. The real numbers shown in (a), (c), (e), and (g) indicate the distances of the selected bonds. The unit is Å.